ORIGINAL ARTICLE

Gastrointestinal lipolysis and trans-epithelial transport of SMEDDS *via* oral route

Fei Xia[a], Zhongjian Chen[b], Quangang Zhu[b], Jianping Qi[a],
Xiaochun Dong[a], Weili Zhao[a], Wei Wu[a], Yi Lu[a*]

[a]*Key Laboratory of Smart Drug Delivery of MOE, School of Pharmacy, Fudan University, Shanghai 201203, China*
[b]*Shanghai Skin Disease Hospital, Tongji University School of Medicine, Shanghai 200443, China*

Abstract   Self-microemulsifying drug delivery systems (SMEDDSs) have recently returned to the lime-light of academia and industry due to their enormous potential in oral delivery of biomacromolecules. However, information on gastrointestinal lipolysis and trans-epithelial transport of SMEDDS is rare. Aggregation-caused quenching (ACQ) fluorescent probes are utilized to visualize the *in vivo* behaviors of SMEDDSs, because the released probes during lipolysis are quenched upon contacting water. Two SMEDDSs composed of medium chain triglyceride and different ratios of Tween-80 and PEG-400 are set as models, meanwhile Neoral® was used as a control. The SMEDDS droplets reside in the digestive tract for as long as 24 h and obey first order kinetic law of lipolysis. The increased chain length of the triglyceride decreases the lipolysis of the SMEDDSs. *Ex vivo* imaging of main tissues and histological examination confirm the trans-epithelial transportation of the SMEDDS droplets. Approximately 2%−4% of the given SMEDDSs are transported *via* the lymph route following epithelial uptake, while liver is the main termination. Caco-2 cell lines confirm the cellular uptake and trans-epithelial transport. In conclusion, a fraction of SMEDDSs can survive the lipolysis in the gastrointestinal tract, permeate across the epithelia, translocate *via* the lymph, and accumulate mainly in the liver.

*Corresponding author. Tel./fax: +86 21 51980084.
E-mail address: fd_luyi@fudan.edu.cn (Yi Lu).

1. Introduction

Self-microemulsifying drug delivery systems (SMEDDSs) are isotropic mixtures of lipids, surfactants and co-solvents, which spontaneously emulsify in gastrointestinal tract (GIT) and arguably form kinetically stable microemulsions[1−3]. For convenience, SMEDDS droplets are referred in the context. Due to the exceptional solvation capability and permeation enhancing effects, SMEDDSs have drawn considerable interests from both academia and industry in improving oral absorption of poorly water-soluble compounds since its introduction in 1980's. The successful commercialization of Sandimmun Neoral® (cyclosporin A), Norvir® (ritonavir), and Fortovase® (saquinavir) inspired further interests in this technology. Within the last five years, numerous discoveries and substantial improvements have been achieved in SMEDDSs, thus bringing this old technology back in the lime light[4].

One of the recent comebacks for SMEDDSs is a game changing approach for oral delivery of hydrophilic peptides, proteins, polysaccharides, and pDNA[5]. A hydrophobic ion pairing technique was developed to incorporate the hydrophilic biomacromolecules in the lipophilic phase of SMEDDSs by complexing them with oppositely charged lipophilic auxiliary agents[6−8]. The microemulsions formed in the GIT protect the cargos from degradation by enzymes and thiol-disulfide exchange with dietary proteins. Mucoadhesive SMEDDSs by incorporating hydrophobic mucoadhesive polymers[9,10], and mucus-penetrating SMEDDSs by PEG-coating[11], mucolytic agents' incorporation[12,13], zeta potential inverting[14], or cell penetrating peptide modification[15,16], have been developed to improve the oral absorption of the macromolecular drugs. The underlying hypothesis is that the drugs are absorbed as the payloads accompanying the translocation of the SMEDDS droplets across the epithelia[5,17]. Although the *in vivo* therapeutic effects confirmed the enhanced absorption of the macromolecular drugs, the intestinal fate of SMEDDSs and the related affecting factors are still unknown[5]. Transwell chamber techniques, rotating silicone tube, fluorescence recovery after photo-bleaching, and multiple particle tracking technique have been exploited to quantify the diffusion of SMEDDS droplets through mucus barriers[17]. However, these techniques ignore the lipid origin of the formulation. Unlike the polymeric nanoparticles, SMEDDSs suffer extensive lipolysis in the GIT. Although the colloidal aspects of dispersion and digestion of SMEDDSs have been well elucidated in *in vitro* lipolysis model[1], the *in vivo* behaviors of SMEDDSs still pose great difficulties to researchers. The fundamental issues concern whether SMEDDSs can survive GI lipolysis and permeate across the epithelia.

Previously, we developed novel aggregation-caused quenching (ACQ) fluorescent probes to track the intact structures of lipid based carriers (LBCs), *e.g.,* solid lipid nanoparticles (SLNs) and nanoemulsions, under lipolysis[18−23]. The probes emit strong near-infrared fluorescence when being molecularly loaded inside the lipid matrix. But the released probes due to lipolysis are completely and instantly quenched upon contacting water. Consequently, the fluorescence of the intact LBCs is discriminated from the buck signals, rendering accurate visualization of the *in vivo* behavior of the carriers[24,25]. The same is true when the probes are dissolved in SMEDDSs. The probes, like drugs, can be encapsulated into the SMEDDS droplets during the self-emulsification process. Thus, the intact SMEDDS droplets can be visualized through the fluorescent signals.

In this study, SMEDDSs composed of Labrafac CC, Tween-80 and PEG-400 with different Tween-80/PEG-400 weight ratios were prepared and set as model samples. Neoral® was set as the control group. ACQ probes, P2 and P4, were loaded for IVIS and confocal laser scan microscope (CLSM) studies, respectively. The purpose is to outline the translocation profiles of oral administered SMEDDSs.

2. Materials and methods

2.1. Materials

Labrafac CC was a kind gift from Gattefosse (Cedex, France), while Tween-80 and PEG-400 were from SINOPHARM (Beijing, China). Neoral® was purchased from Novartis (Basel, Switzerland). DAPI (4′,6-diamidino-2-phenylindole) and optimal cutting temperature (OCT) compound was from Shanghai Yeasen Biotech (Shanghai, China) and Leica (Mannheim, Germany), respectively. DMEM, RPMI 1640 and fetal bovine serum are from Gibco Invitrogen (Carlsbad, CA, USA). Caco-2 (human colorectal adenocarcinoma cell) and Raji (human Burkitt's lymphoma cell) were obtained from the Cell Bank of the Chinese Academy of Sciences (Shanghai, China), while HT29-MTX cells were from China Center for Type Culture Collection (Wuhan, China). The ACQ probes, known as P2 and P4, were synthesized in the laboratory[26].

Sprague−Dawley (SD) rats (male, 200 ± 20 g) were provided by SLAC Laboratory Animal (Shanghai, China). The procedures of animal experimental were approved by the Committee on Welfare and Ethics of Experimental Animals at School of Pharmacy, Fudan University, China.

2.2. SMEDDS preparation

Table 1 shows the formulation of the SMEDDSs. Two SMEDDSs were prepared with varied Tween-80/PEG-400 ratios and encoded S1 and S2 (Supporting Information Fig. S1), respectively. For loading of the ACQ probes, 100 μL dichloromethane containing 100 μg P2 or 20 μg P4 was put in glass tube. Dichloromethane was removed under nitrogen sweeping. PEG-400 was added in the tube, which was violently vibrated under vortex till the probe residues were dissolved. Finally, Labrafac CC and Tween-80 were added and mixed with PEG-400 homogeneously under vortex.

Preparation of P2/P4-loaded Neoral® was similar to that of the SMEDDS formulations. The oil content was collected from the soft capsules of Neoral®. Then, 100 μg P2 or 20 μg P4 was dissolved in 1 g of the content under vortex.

The SMEDDS formulations were dispersed in 8-fold of pure water under vortex for characterization and cellular studies.

2.3. Characterization

Zetasizer Nano (Malvern Panalytical, Malvern, UK) was used to measure the particle size, polydispersity index (PDI) and Zeta-potential. Transmission electron microscope (TEM, JEOL Ltd., JEM-1230, Tokyo, Japan) was used to observe the morphology. IVIS Spectrum (PerkinElmer, Waltham, MA, USA) was adopted to measure the fluorescent intensity of P2 (λ_{abs}, 710 nm; λ_{em}, 760 nm) and P4 (λ_{abs}, 640 nm; λ_{em}, 680 nm), being expressed as average radiant efficiency (ARE) by a region of interest (ROI) quantification method.

Table 1 Formulation and characterization of S1, S2 and Neoral®.

SMEDDS	Formulation weight (g)			Water (mL)	Size (nm)[a]	PDI[a]	ζ (mV)[a]	P2/P4 (μg)	Fluorescence intensity (TRE, $\times 10^{-10}$)[a]
	Labrafac CC	Tween-80	PEG-400						
P2@S1	0.10	0.45	0.45	8	19.06 ± 1.07	0.13 ± 0.03	-3.10 ± 0.21	100	1.14 ± 0.14
P4@S1								20	9.51 ± 0.11
P2@S2	0.10	0.30	0.60	8	26.31 ± 0.74	0.16 ± 0.02	-2.75 ± 0.54	100	1.11 ± 0.25
P4@S2								20	9.43 ± 0.21
P2@Neoral®		1.00		8	30.80 ± 1.04	0.08 ± 0.01	-1.76 ± 0.42	100	1.11 ± 0.26
P4@Neoral®								20	9.12 ± 0.43

SMEDDS, self-microemulsifying drug delivery systems; PDI, polydispersity index; TRE, total radiant efficiency.
[a]Data are presented as mean $\pm$ SD ($n = 3$).

2.4. Fluorescent stability

The SMEDDSs, 0.8 g, was homogeneously dispersed in 6 mL deionized water or buffers of different pHs for self-microemulsification. The dispersions were incubated at 37 °C for 24 h. Before and 4, 8, 12, and 24 h after the incubation, samples were withdrawn for size, PDI, and fluorescent intensity measurement.

2.5. Gastrointestinal lipolysis

As proved in previous studies, the decrease of fluorescent intensity correlated very well with the lipolysis of lipid-based formulations, while IVIS (PerkinElmer) provides a real-time monitor for the *in vivo* lipolysis process[19–23]. The SMEDDSs, 1 g, were given by gavage to each rat. At predetermined intervals, the rats were anaesthetized with isoflurane using an on-line gas anesthetizing system for IVIS Live Imaging. The ARE values within the ROIs were measured by vendor software for subsequent quantitative analysis.

2.6. Gastrointestinal translocation and in vivo distribution

After gavage of 1 g SMEDDSs, 100 μL venous blood was collected from the eye socket of the rats at predetermined intervals. Then the rats were sacrificed by overdose of pentobarbital sodium (i.p.). The whole GIT and main tissues (*i.e.*, liver, lung, spleen, and kidneys) were then dissected and visualized under IVIS (PerkinElmer). The total radiant efficiency (TRE) values of the ROIs were measured.

2.7. Trans-epithelial transportation

Histological examination of the jejunum segment following in situ single-pass intestinal perfusion was performed to investigate the trans-epithelial transportation of the SMEDDSs[19]. Briefly, the jejunum segment was cannulated to form a loop, where the SMEDDSs were perfused from the pylorus to the ileum until an equilibrium of fluorescent intensity in the effluents was achieved. Then the jejunum segment was successively excised, fixed in 4% paraformaldehyde solution, dehydrated in 30% sucrose solution and frozen in the OCT compound. The frozen tissues were cut into 10 μm slices, which were stained with DAPI and observed under CLSM (Carl Zeiss Inc., LSM710, Jena, Germany).

2.8. Lymphatic transportation

Lymphatic transport of the SMEDDSs was studied in conscious rat with mesenteric lymphatic cannulation. Male SD rats weighing 300–350 g were fed with 1.5 mL peanut oil 30 min before the surgery. Then the rats were anesthetized by intraperitoneal injection of 50 mg/kg sodium pentobarbitone. The mesenteric lymph duct was cannulated with a polyethylene tube (Instech Laboratories Inc., PE-25, Plymouth Meeting, PA, USA) as described previously[27,28]. The animals were fasted while with free access to Ringer's solution for recovering overnight (12–18 h). After oral administration of the SMEDDSs *via* gavage, lymph samples were collected continuously until 36 h post oral administration. The cumulative P2 fluorescence (TRE) in the lymph fluids was measured using the IVIS (PerkinElmer). For quantification, the SMEDDSs were diluted with blank lymph fluids to get lymph samples with a series concentrations of SMEDDS. The fluorescent intensities of these samples were measured with IVIS (PerkinElmer) to establish calibration curves for the amount of the SMEDDS. Within the concentration range from 1.56×10^{-4} to 1×10^{-2} (mg/mg), good linear relationships are found with the TRE values, while the within- and inter-day precisions are all below 2%.

2.9. Cellular interaction

Cell culture was performed following previously established procedures[20,29]. Cellular uptake was performed on Caco-2 and Caco-2/HT29-MTX co-culture monolayers. Caco-2 cells in density of $5 \times 10^4/cm^2$ were seeded and cultured for 14 days under 5% CO_2, 90% relative humidity, and at 37 °C. For co-culture monolayers, Caco-2 and HT29-MTX cells were mixed at a population ratio of 7:3 and seeded in a total density of 1×10^5 cells/cm². Due to lack of agitation, 200 μL aqueous dispersion of the SMEDDSs was added to the cell model and incubated for 2 h. Following washing with PBS, the cells were recorded by IVIS and observed under CLSM (Carl Zeiss Inc.) following DAPI staining, respectively.

Caco-2/HT29-MTX and Caco-2/HT29-MTX/Raji cell models were cultured to investigate the trans-monolayer transport of the SMEDDSs. Caco-2 and HT29-MTX (7:3) mixed cells were seeded in a total density of 1×10^5 cells per cm² onto the apical (AP) side of Millicell® inserts (Millipore, Billerica, MA, USA) and cultured for 21 days. A Millicell ERS-2 (Millipore, Billerica, MA, USA) was used to monitor the trans-epithelial electrical resistance (TEER) of cell monolayers. A TEER of 300 $\Omega \cdot cm^2$ confirms the formation of tight junctions, *i.e.*, an integral cell monolayer. For Caco-2/HT29-MTX/Raji cell model, the initial culturing is the same with that used in the Caco-2/HT29-MTX cell model until the formation of tight junctions. Raji cells were added to the basolateral (BL) side and co-cultured for another 4–5 days for infiltration, which is indicated by a drop of TEER value below
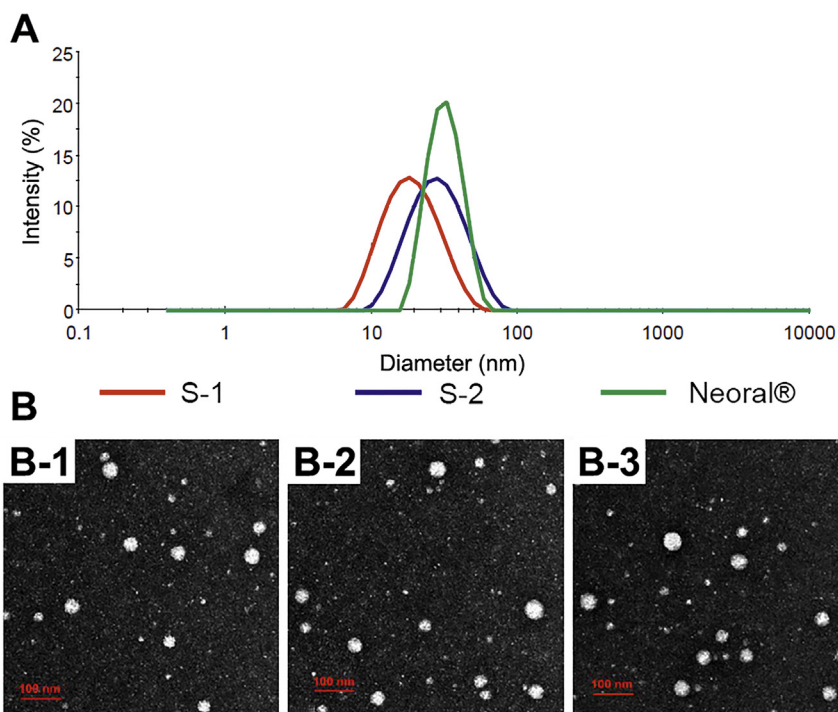
Figure 1 Size distribution (A) and TEM pictures (B) of S1 (B-1), S2 (B-2) and Neoral® (B-3) (scale bar = 100 nm).
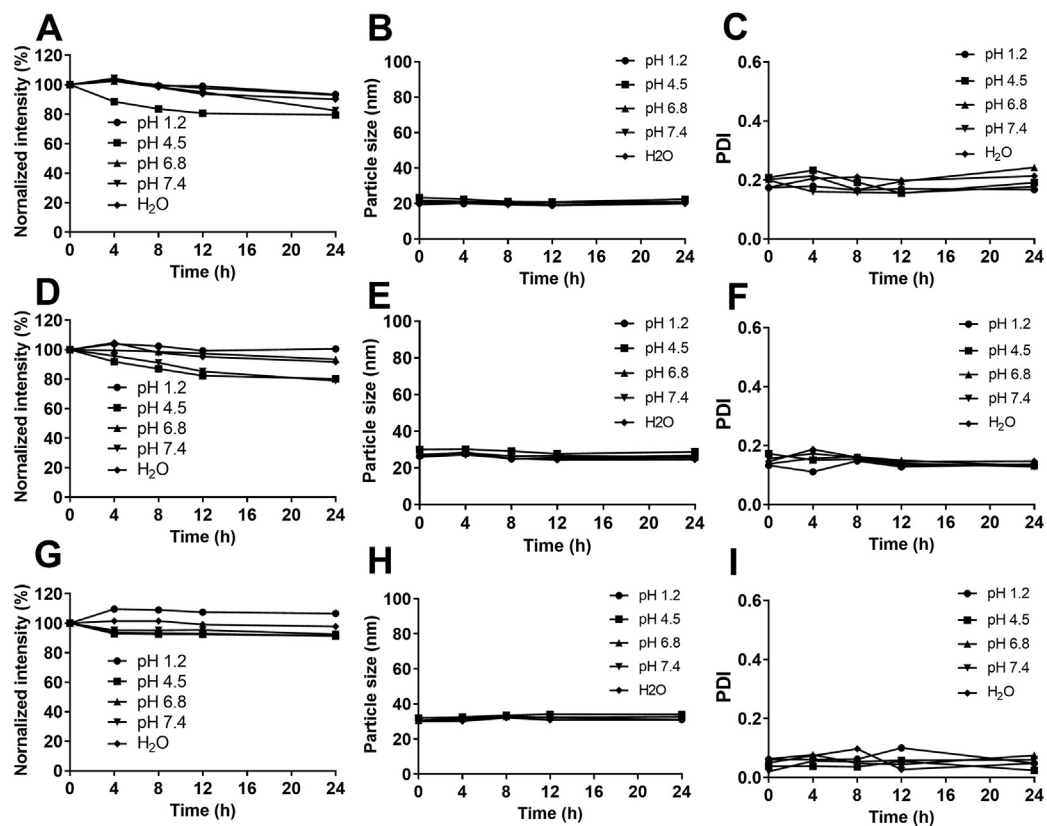

Figure 2 Stability of fluorescent intensity (A, D, G), particle size (B, E, H) and PDI (C, F, I) of S1 (A, B, C), S2 (D, E, F) and Neoral® (G, H, I) in water and buffers of different pHs.

250 $\Omega \cdot cm^2$. Then 200 μL aqueous dispersion of the SMEDDSs was added to the AP side, while 600 μL HBSS to the BL side of the insert. At 1, 2, and 4 h of incubation at 37 °C, 200 μL samples were withdrawn for measurement of fluorescent intensity.

2.10. Statistical analysis

One-way analysis of variance (ANOVA) was applied to test for significance in the experiments. Statistical significance was set at $P < 0.05$.

3. Results and discussions

3.1. Characterization of the SMEDDSs

The appearance of the aqueous dispersion of blank and P2/P4-loaded SMEDDSs is shown in Supporting Information Fig. S2. All the dispersions are transparent with light blue opalescence. Loading of probes doesn't change the appearance of the dispersions but slightly burns the colors. The size of the SMEDDSs varies between 19 nm and 30 nm with a normal distribution, while the PDIs are all less than 0.20 (Table 1 and Fig. 1A). The morphology of the dispersed SMEDDSs is spherical, while the observed size distribution is coincident with results from

Zetasizer Nano (Fig. 1B). Besides, the zeta potential and the fluorescent intensity were comparable among SMEDDSs (Table 1).

3.2. Fluorescent stability

An accurate imaging requires a stable fluorescence from the carriers and absence of fluorescent recurrence due to dissolving of aggregated probes by endogenous solubilizers such as phospholipids and bile salts[30−33]. Negligible interferences from fluorescent recurrence have been confirmed previously with quenched aqueous solution of the ACQ probes as a control group[19−23]. The *in vivo* and *ex vivo* experiments in this study follow the same dosage and procedures as that used in the previous ones. However, since a different LBC was investigated, the stability of fluorescently labeled SMEDDSs was studied (Fig. 2). The particle size (Fig. 2B, E, and H) and the PDI value (Fig. 2C, F, and I) are rather stable in all media, indicating stable and intact structures. The fluorescent intensities of S1 and S2 in pH 4.5 acetate buffers get a slight decrease, while a slight increase for Neoral® in pH 1.2 hydrochloric acid solution is seen (Fig. 2A, D, and G). The fluctuation of the fluorescent intensity may be due to the variation[34−36]. Generally, the fluorescence of the SMEDDSs is stable in aqueous media. Fluorescent quenching due to either probe
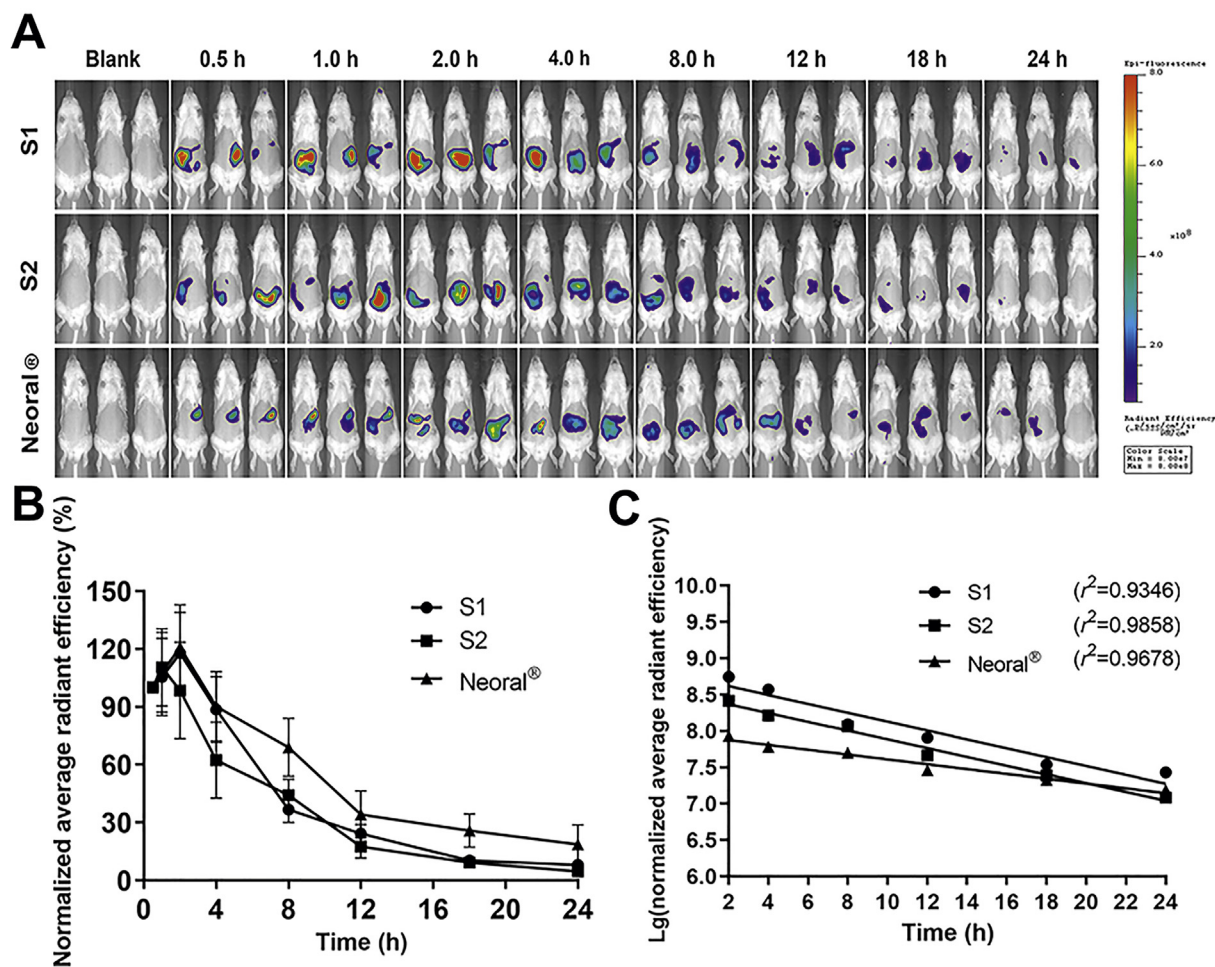

Figure 3   Live imaging photographs in rats after gavage administration of S1, S2 and Neoral® (A). Quantification plots of fluorescent intensity (average radiant efficiency) in rats *vs.* time; Data are presented as mean ± SD ($n = 3$) (B). The plots fit to first-order kinetic law (C).
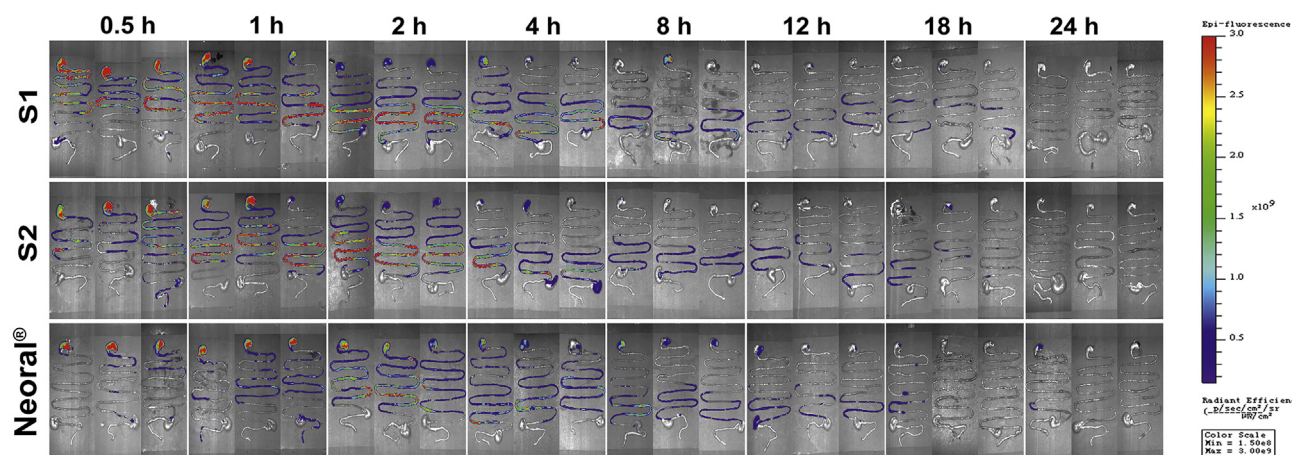
Figure 4   *Ex vivo* imaging of the whole dissected GIT after gavage administration of S1, S2 and Neoral®.

leakage or water infiltration is negligible. The fluorescence can be used to monitor the structural change of the SMEDDSs.

3.3.   In vivo lipolysis

The live imaging of the rats before and after being given P2 labeled SMEDDSs is shown in Fig. 3A. All SMEDDSs show a long residence in the GIT up for 24 h with a gradual decreasing trend of fluorescence. Compared with the quick lipolysis of SLNs (4 h)[21], the lipolysis of SMEDDSs is rather slow. More particles may survive the lipolysis and have chances to interact with the epithelia[22]. Though being limited in knowledge, the slow lipolysis may be due to the extremely small particle size of the SMEDDSs. Both *in vitro* and *in vivo* studies have shown slowing down lipolysis of nanoemulsions at decreased particle size from 550 to 80 nm[19]. The finding is contradictory to the existing knowledge that increased specific surface from the reduced size facilitates reactions[37,38]. The underlying mechanisms are yet to be explored.

The *in vivo* lipolysis is displayed as the normalized ARE values *vs.* time, and the initial fluorescence intensity is set as 100% (Fig. 3B). All SMEDDSs present similar trends in kinetics. A slight increase in the fluorescent signals is seen in the first 2 h. Then the fluorescence declines gradually to a low level at 24 h. The initial increase of fluorescence may be due to the dispersion and self-microemulsification process. Neoral® presents higher normalized ARE values than the other two SMEDDSs during the lipolysis process, indicating slower *in vivo* lipolysis. The differences are mainly ascribed to the chain length of the lipids. Medium-chain triglycerides (MCTs), *i.e.*, Labrafac CC, were used in S1 and S2, while long-chain triglycerides (LCTs), *i.e.*, corn oil, were used in Neoral®[39]. A faster lipolysis rate was found in MCTs than in LCTs[40−42]. Due to the same amount of Labrafac CC, S1 and S2 demonstrate similar behavior in the mid-posterior stage of the lipolysis. However, the Tween-80/PEG-400 ratio has certain effects on the initial stage of dispersion. Starting from 2 h post administration, the *in vivo* lipolysis profiles can be well fitted to first-order kinetics (Fig. 3C). A lipolysis half-life of 4.94, 4.99, and 9.06 h are calculated for S1, S2, and Neoral®, respectively.

3.4.   GI retention

Fig. 4 shows the *ex vivo* imaging of the whole GIT of rats treated with SMEDDSs. All the SMEDDSs show similar GI transport and retention. Until 24 h post administration, faint fluorescence is seen, indicating long residence of SMEDDSs in the GIT. The gastric emptying of the SMEDDSs is quick, because fluorescent signals appear in the small intestine at 0.5 h. This may be ascribed to the extremely small size of the SMEDDSs. At 2 h, the SMEDDSs have been transported throughout the small intestines. This finding confirms the resistance of the SMEDDSs to lipases. Conversely, SLN signals can only be found in the stomach due to the intense lipolysis in the small intestine[20]. Slowing down the lipolysis by PEG coating or lipase inhibitor facilitates the survival of SLNs in the intestine[22].

3.5.   In vivo distribution

Fig. 5A shows the *ex vivo* imaging of primary organs of the rats treated by the SMEDDSs. Strong fluorescent signals are seen in various organs after 2 h, confirming the absorption of intact SMEDDS droplets that survive the lipolysis in the GIT. Considering the appearance time and the intensity of the fluorescence, liver is the main accumulation organ, followed by the lung, the spleen and the kidney. Quantification of total fluorescence in the liver along with the time is performed and shown in Fig. 5B. All SMEDDSs present similar liver exposure based on the area under the curve (AUC), which is 4.72×10^{11}, 4.73×10^{11} and 4.36×10^{11} for S1, S2, and Neoral®, respectively. In the initial 4 h, the accumulation rate and amount in the liver is in the sequence of S1>S2> Neoral®, which may be due to the different absorption rates. The peak times for each SMEDDSs are far behind their transportation in the GIT, being 18 h for S1 and S2, 12 h for Neoral®, respectively. This may be due to the long absorption process. Nonetheless, the maximum fluorescent intensities are comparable among the three formulations.

3.6.   Pharmacokinetics in blood and lymphatic transport

Fig. 6A shows the variation of fluorescent intensity in blood post administration of the SMEDDSs. The fluorescent intensities in the blood are generally one thousandth that in the liver, because nanoparticles in blood circulation are rapidly captured by the liver[43]. The initial absorption of the SMEDDSs is in the sequence of S1>S2>Neoral®. A 1-h lag of absorption is found for Neoral® comparaed with S1 and S2. These results explain the initial differences in liver accumulation among the formulations.

Nonetheless, Neoral® shows a more sustained absorption than S1 and S2, presenting a peak time of 18 h *versus* 12 h of S1 and 8 h of S2. Superior lipolysis resistance from LCT to MCT is the main reason for the different absorption patterns. Minute disparities in the AUCs are found among the formulations, which are 3.40×10^8, 2.57×10^8 and 2.68×10^8 for S1, S2 and Neoral®, respectively. However, due to the faint fluorescent intensity in comparison with that in the liver, it is not rational to compare the bioavailability of SMEDDSs using the AUC values in the blood.

Fig. 6B shows the cumulative transfer percentage of SMEDDSs *via* the lymphatic route in rats. SMEDDS signals appear in the lymph at 2 h post administration and go steadily up at the first 12 h. The cumulative lymphatic transportation is similar for S1 and S2, being $3.96 \pm 0.98\%$ and $4.20 \pm 1.30\%$ at 36 h, respectively. Neoral® gets a comparatively lower lymphatic transportation of $2.03 \pm 0.43\%$ than S1 and S2. Since the particle sizes of the SMEDDSs are similar, the differences may be due to the compositions. We once studied the lymphatic transportation of intact nanoemulsions and polymeric nanoparticles[17,31]. In the size range from 50 to 1000 nm, the lymphatic transportation of intact carriers is increased with size reduction. The maximum value is $5.94 \pm 1.02\%$ from 80 nm nanoemulsions and $2.39 \pm 1.81\%$ from

50 nm polymeric nanoparticles[19,36]. However, the smaller SMEDDSs doesn't produce higher lymphatic transportation than the larger nanoemulsions and polymeric nanoparticles. Besides size and composition, factors affecting lymphatic transportation of SMEDDSs are yet to be explored.

3.7. Trans-epithelial transportation

In order to provide concrete evidence supporting the absorption of intact SMEDDS droplets, the jejunum of the rat treated by *in-situ* perfusion was sliced and observed under CLSM (Carl Zeiss Inc., Fig. 7). The red fluorescence represents the intact SMEDDS droplets while the blue one indicates the cell nucleus. Red fluorescence can be seen in the whole villi and co-localize well with the blue signal. The intensity of the co-localized signals, *i.e.*, the purple, decrease from the epithelium to the lamina propria, supporting the trans-epithelial transportation of the intact SMEDDS droplets. Since abundant networks of lymphatic and blood capillaries reside in the lamina propria, the intact SMEDDS droplets have good chances to be absorbed *via* either the blood or the lymph. Generally, nanoparticles in the interstitial fluid are primarily absorbed *via* the lymph due to the
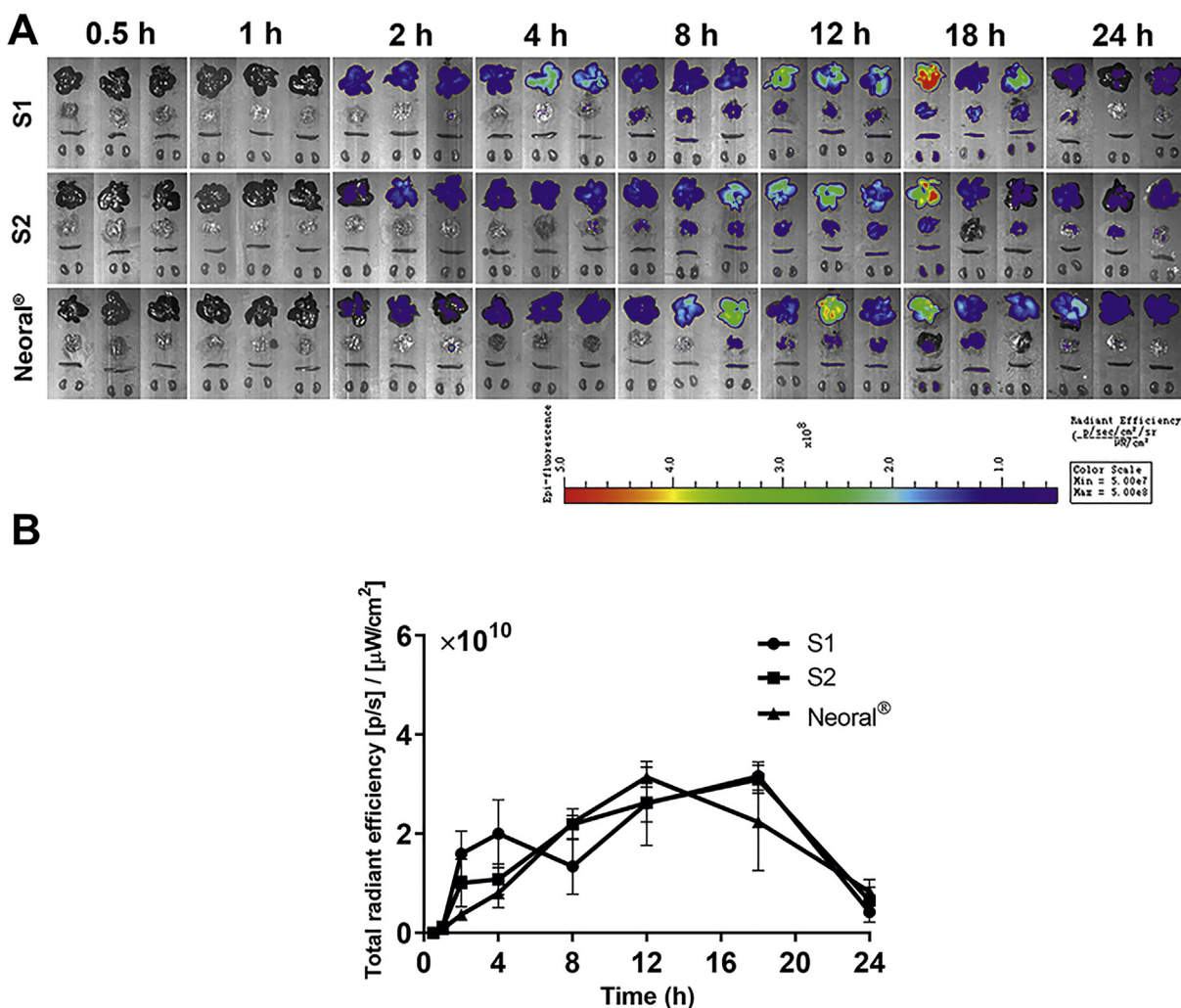

Figure 5 *Ex vivo* imaging of dissected organs after gavage administration of S1, S2 and Neoral® (A) and fluorescence intensity *vs.* time plots in the liver; Data are presented as mean ± SD ($n = 3$) (B).
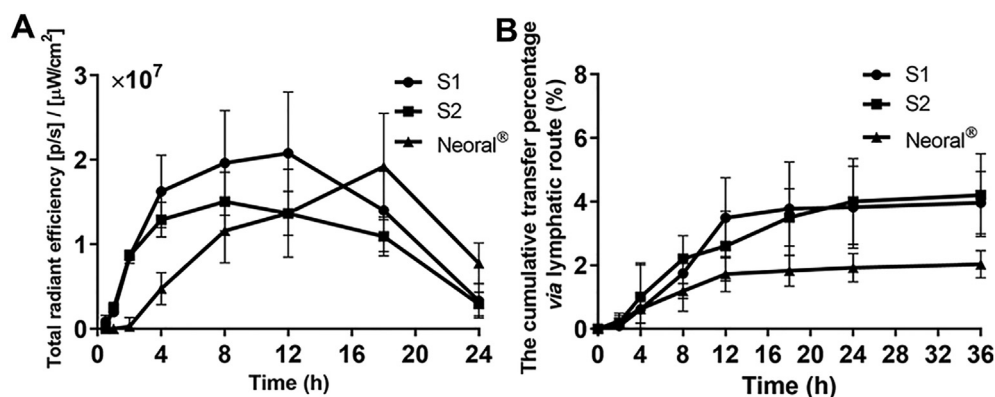
Figure 6 Pharmacokinetics in blood presented as total radiant efficiency of blood-borne fluorescence *vs.* time (A); cumulative transport percentage of SMEDDSs *via* lymph (B). Data are presented as mean ± SD ($n = 3$).

large openings in the lymphatic vessels[44]. The lymph vessels are incorporated into the thoracic duct or ductus lymphaticus dexter and join in the blood circulation. The slow lymph flow may lead to steady plasma concentration and prolong the peak time. Due to the huge differences in flow velocity between lymph and blood circulation as well as the rapid elimination by macrophages, SMEDDSs transported to the blood are quickly accumulated in the liver, while the peak time is postponed, ranging from 8 to 18 h.

3.8. Cellular uptake

Caco-2 and Caco-2/HT29-MTX cell models were used to perform the cellular uptake of the SMEDDSs. The co-culture model was used to evaluate the effects of mucus on the absorption of the SMEDDSs[32,45]. The fluorescence images and quantification of the

cellular uptake of the SMEDDSs are shown in Fig. 8A and B. Visual observation of the fluorescence images and statistical analysis of the fluorescent intensities give no differences in cellular uptake among the SMEDDSs. Of note is that lipolysis of the SMEDDSs is absent in the cellular study due to free of lipases in the culture medium. The similar particle sizes and zeta potentials account for the similar cellular uptakes. Moreover, due to the advantages of small particle size to the mucosal penetration[46,47], no significant differences are found in cellular uptakes between the two cell models.

Location of the SMEDDSs during the trans-monolayer transportation was further explored by CLSM (Carl Zeiss Inc.). The red signals represent the intact SMEDDSs while the blue ones are the cell nucleus. Co-localization of the red and the blue signals in the X-Z plane scanning confirms the uptake of the intact SMEDDSs. Besides, the Z axis scanning reveals red signals in the basolateral side of the cell monolayer, supporting the trans-epithelial transport
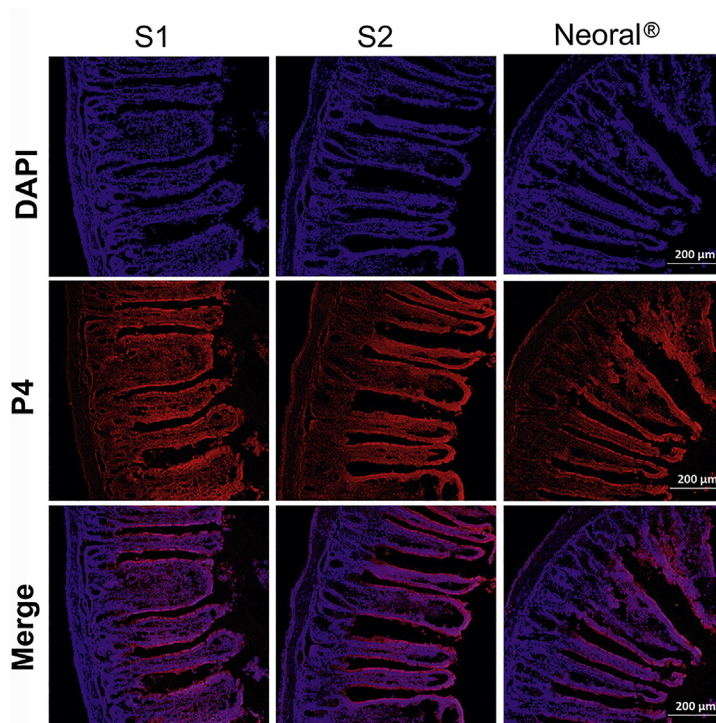

Figure 7 CLSM images of frozen section of jejunum segments after in situ perfusion with S1, S2 and Neoral® (scale bar = 200 μm).
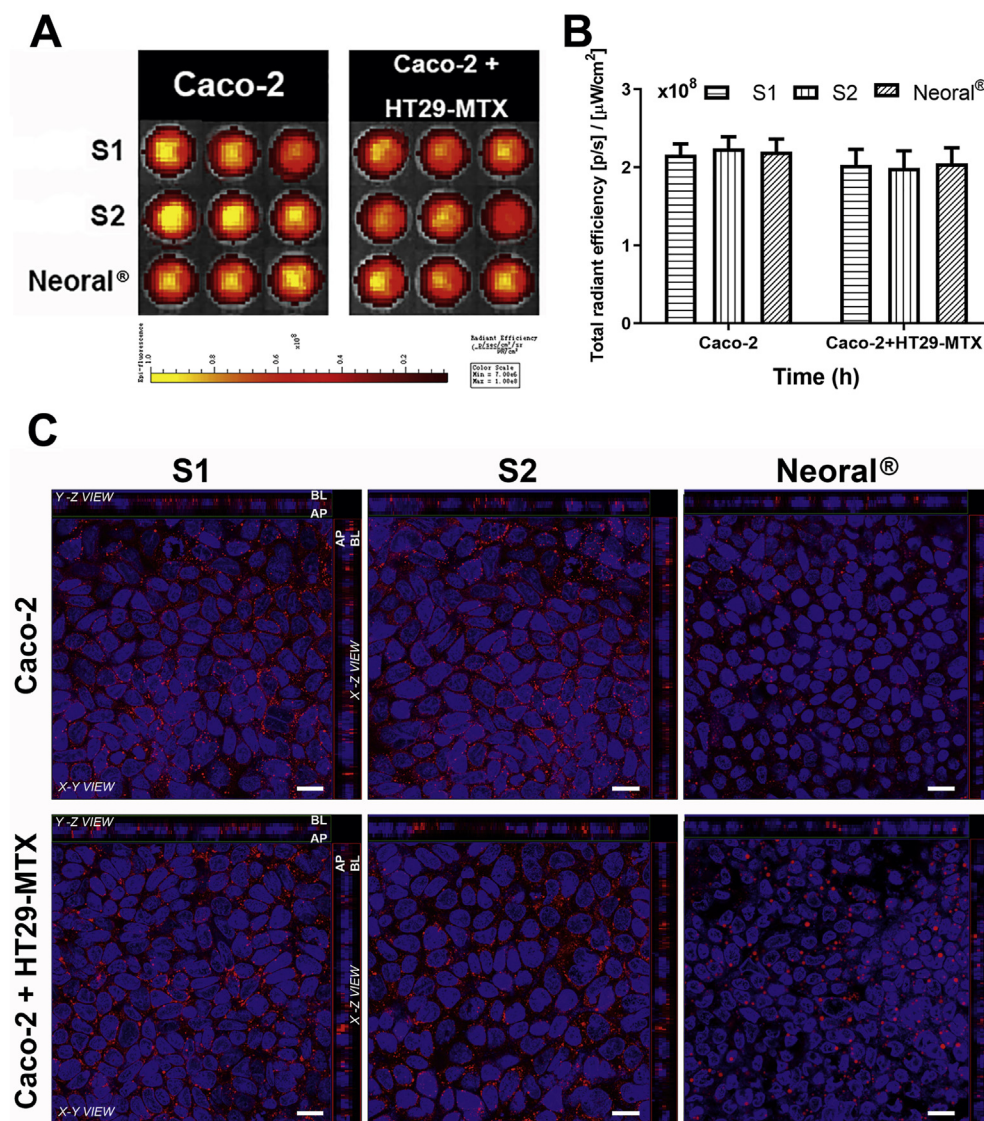
Figure 8 Cellular uptake of the SMEDDSs. Live images (A) and quantification (B) of cellular uptake by Caco-2 and Caco-2+HT29-MTX cell lines. CLSM images of cell monolayers visualize the internalization of the SMEDDSs (scale bar = 20 μm) (C).
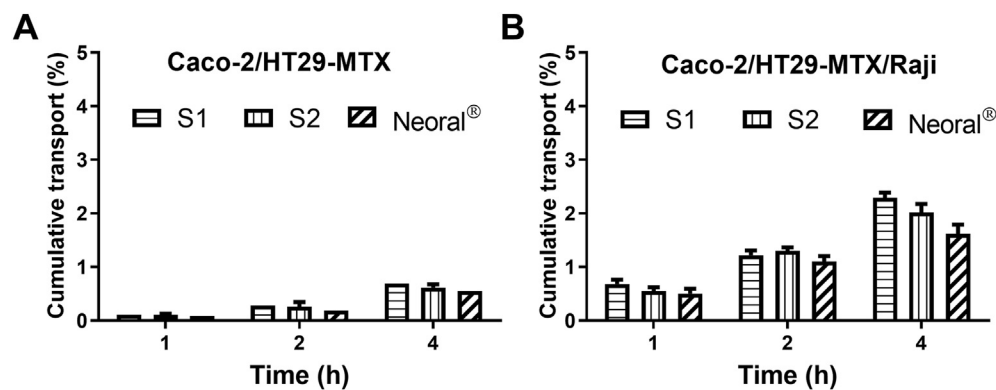

Figure 9 Cumulative transport *vs.* time of SMEDDSs across Caco-2+HT29-MTX (A) and Caco-2+HT29-MTX + Raji (B) cell monolayers. Data are presented as mean ± SD (*n* = 3).

of the intact SMEDDSs. Similar results obtained from the Caco-2 and the Caco-2/HT29-MTX models again prove the good mucosal penetrating capability of the SMEDDSs.

3.9. Transmembrane transportation

Caco-2/HT29-MTX and Caco-2/HT29-MTX/Raji cell models were further used to study the transmonolayer transport of the SMEDDSs (Fig. 9). Co-culturing with Raji cells mimics M cells. Appearance of P4 signal at the BL side confirms trans-monolayer transport of intact SMEDDSs. Besides, the intensity of P4 signals increase with time in both cell models. In Caco-2/HT29-MTX co-culture model, the cumulative trans-monolayer transports at 4 h are similar among S1, S2 and Neoral®, which are $0.70 \pm 0.05\%$, $0.61 \pm 0.06\%$ and $0.55 \pm 0.10\%$, respectively. Due to the strong transcytotic capacities of M cells to transport particulate materials[48−50], almost double increases in cumulative trans-monolayer transports are obtained in Caco-2/HT29-MTX/Raji co-culture model, i.e., $2.29 \pm 0.10\%$, $2.02 \pm 0.16\%$ and $1.62 \pm 0.17\%$ for S1, S2 and Neoral®, respectively. Neoral® shows a slightly lower trans-monolayer transportation than both S1 and S2. The exact mechanisms are not well known.

4. Conclusions

The ACQ probes render the visualization of the *in vivo* lipolysis and transport of intact SMEDDS droplets. SMEDDSs reside in the GIT of rats for up to 24 h, although they suffer lipolysis in a first order kinetic model. The SMEDDSs consisting of LCT have a slightly higher resistance to the lipolysis than the ones consisting of MCT. The survival SMEDDS droplets can permeate across the epithelia, where they are transported *via* either the blood or the lymph ducts. Around 2%−4% administered SMEDDSs are transported *via* the lymphatic route. The SMEDDSs in the circulation are delivered to several organs with the liver as the major accumulating organ. *In vitro* Caco-2 cell models confirm the uptake and trans-monolayer transfer of the intact SMEDDS droplets. It is concluded that SMEDDSs are potential for oral delivery of labile entities as they can transport across the enterocytes and enter the circulation.

Acknowledgments

Author contributions

Weili Zhao, Wei Wu and Yi Lu designed the research. Fei Xia carried out the experiments and performed data analysis. Zhongjian Chen, Quangang Zhu, Jianping Qi and Xiaochun Dong participated part of the experiments. Yi Lu wrote the manuscript. All of the authors have read and approved the final manuscript.

Conflicts of interest

The authors have no conflicts of interest to declare.

Appendix A.   Supporting information

Supporting data to this article can be found online at https://doi.org/10.1016/j.apsb.2021.03.006.

References

1. Vithani K, Jannin V, Pouton CW, Boyd BJ. Colloidal aspects of dispersion and digestion of self-dispersing lipid-based formulations for poorly water-soluble drugs. *Adv Drug Deliv Rev* 2019;**142**:16−34.
2. Kuentz M. Drug supersaturation during formulation digestion, including real-time analytical approaches. *Adv Drug Deliv Rev* 2019;**142**:50−61.
3. Tao C, Yu Y, Chen ZZ, Zhang MX, Liu LL, Liu ZH, et al. Effect of mesopores on solidification of sirolimus self-microemulsifying drug delivery system. *Chin Chem Lett* 2018;**29**:1849−52.
4. Bernkop-Schnurch A, Mullertz A, Rades T. Self-emulsifying drug delivery systems (SEDDS)—the splendid comeback of an old technology. *Adv Drug Deliv Rev* 2019;**142**:1−2.
5. Mahmood A, Bernkop-Schnurch A. SEDDS: a game changing approach for the oral administration of hydrophilic macromolecular drugs. *Adv Drug Deliv Rev* 2019;**142**:91−101.
6. Griesser J, Hetenyi G, Moser M, Demarne F, Jannin V, Bernkop-Schnurch A. Hydrophobic ion pairing: key to highly payloaded self-emulsifying peptide drug delivery systems. *Int J Pharm* 2017;**520**:267−74.
7. Bonengel S, Jelkmann M, Abdulkarim M, Gumbleton M, Reinstadler V, Oberacher H, et al. Impact of different hydrophobic ion pairs of octreotide on its oral bioavailability in pigs. *J Control Release* 2018;**273**:21−9.
8. Zupancic O, Griebetainger JA, Rohrer J, Pereira de Sousa I, Danninger L, Partenhauser A, et al. Development, *in vitro* and *in vivo* evaluation of a self-emulsifying drug delivery system (SEDDS) for oral enoxaparin administration. *Eur J Pharm Biopharm* 2016;**109**:113−21.
9. Leonaviciute G, Adamovic NT, Lam HT, Rohrer J, Partenhauser A, Bernkop-Schnürch A. Self-emulsifying drug delivery systems (SEDDS): proof-of-concept how to make them mucoadhesive. *Eur J Pharm Biopharm* 2017;**112**:51−7.
10. Hetenyi G, Griesser J, Nardin I, Bernkop-Schnurch A. Combination of SEDDS and preactivated thiomer technology: incorporation of a preactivated thiolated amphiphilic polymer into self-emulsifying delivery systems. *Pharm Res (N Y)* 2017;**34**:1171−9.
11. Inchaurraga L, Martin-Arbella N, Zabaleta V, Quincoces G, Penuelas I, Irache JM. *In vivo* study of the mucus-permeating properties of PEG-coated nanoparticles following oral administration. *Eur J Pharm Biopharm* 2015;**97**:280−9.
12. Leichner C, Menzel C, Laffleur F, Bernkop-Schnurch A. Development and *in vitro* characterization of a papain loaded mucolytic self-emulsifying drug delivery system (SEDDS). *Int J Pharm* 2017;**530**:346−53.
13. Efiana NA, Phan TNQ, Wicaksono AJ, Bernkop-Schnurch A. Mucus permeating self-emulsifying drug delivery systems (SEDDS): about the impact of mucolytic enzymes. *Colloids Surf B Biointerfaces* 2018;**161**:228−35.
14. Suchaoin W, Pereira de Sousa I, Netsomboon K, Lam HT, Laffleur F, Bernkop-Schnurch A. Development and *in vitro* evaluation of zeta potential changing self-emulsifying drug delivery systems for enhanced mucus permeation. *Int J Pharm* 2016;**510**:255−62.
15. Mahmood A, Prufert F, Efiana NA, Ashraf MI, Hermann M, Hussain S, et al. Cell-penetrating self-nanoemulsifying drug delivery systems (SNEDDS) for oral gene delivery. *Expet Opin Drug Deliv* 2016;**13**:1503−12.
16. Sun M, Hu HK, Sun LM, Fan Z. The application of biomacromolecules to improve oral absorption by enhanced intestinal permeability: a mini-review. *Chin Chem Lett* 2020;**31**:1729−36.

17. Abdulkarim M, Sharma PK, Gumbleton M. Self-emulsifying drug delivery system: mucus permeation and innovative quantification technologies. *Adv Drug Deliv Rev* 2019;**142**:62−74.

18. Qi JP, Hu XW, Dong XC, Lu Y, Lu HP, Zhao WL, et al. Towards more accurate bioimaging of drug nanocarriers: turning aggregation-caused quenching into a useful tool. *Adv Drug Deliv Rev* 2019;**143**:206−25.

19. Xia F, Fan WF, Jiang SF, Ma YH, Lu Y, Qi JP, et al. Size-dependent translocation of nanoemulsions *via* oral delivery. *ACS Appl Mater Interfaces* 2017;**9**:21660−72.

20. Hu XW, Fan WF, Yu Z, Lu Y, Qi JP, Zhang J, et al. Evidence does not support absorption of intact solid lipid nanoparticles *via* oral delivery. *Nanoscale* 2016;**8**:7024−35.

21. Hu XW, Zhang J, Yu Z, Xie YC, He HS, Qi JP, et al. Environment-responsive aza-BODIPY dyes quenching in water as potential probes to visualize the *In vivo* fate of lipid-based nanocarriers. *Nanomed* 2015;**11**:1939−48.

22. Yu Z, Fan WF, Wang LT, He HS, Lv YJ, Qi JP, et al. Slowing down lipolysis significantly enhances the oral absorption of intact solid lipid nanoparticles. *Biomater Sci* 2019;**7**:4273−82.

23. Yu Z, Fan WF, Wang LT, Qi JP, Lu Y, Wu W. Effect of surface charges on oral absorption of intact solid lipid nanoparticles. *Mol Pharm* 2019;**16**:5013−24.

24. Yang JL, Dong ZR, Liu WJ, He HS, Fan WF, Lu Y, et al. Discriminating against injectable fat emulsions with similar formulation based on water quenching fluorescent probe. *Chin Chem Lett* 2020;**31**:875−9.

25. Liu DL, Wan B, Qi JP, Dong XC, Zhao WL, Wu W, et al. Permeation into but not across the cornea: bioimaging of intact nanoemulsions and nanosuspensions using aggregation-caused quenching probes. *Chin Chem Lett* 2018;**29**:1834−8.

26. Zhao W, Carreira EM. Conformationally restricted aza-bodipy: a highly fluorescent, stable, near-infrared-absorbing dye. *Angew Chem Int Ed* 2005;**44**:1677−9.

27. Xie YC, Jiang SF, Xia F, Hu XW, He HS, Yin ZN, et al. Glucan microparticles thickened with thermosensitive gels as potential carriers for oral delivery of insulin. *J Mater Chem B* 2016;**4**:4040−8.

28. Guan PP, Lu Y, Qi JP, Wu W. Readily restoring freeze-dried probilosomes as potential nanocarriers for enhancing oral delivery of cyclosporine A. *Colloids Surf, B* 2016;**144**:143−51.

29. Zhao SN, Li JH, Wang FZ, Yu T, Zhou Y, He LL, et al. Semi-elastic core−shell nanoparticles enhanced the oral bioavailability of peptide drugs. *Chin Chem Lett* 2020;**31**:1147−52.

30. Yang YQ, Lv YJ, Shen CY, Shi TT, He HS, Qi JP, et al. *In vivo* dissolution of poorly water-soluble drugs: proof of concept based on fluorescence bioimaging. *Acta Pharm Sin B* 2020. Available from: https://doi.org/10.1016/j.apsb.2020.08.002.

31. Ahmad E, Lv YJ, Zhu QG, Qi JP, Dong XC, Zhao WL, et al. TAT modification facilitates nose-to-brain transport of intact mPEG-PDLLA micelles: evidence from aggregation-caused quenching probes. *Appl Mater Today* 2020;**19**:100556.

32. He HS, Wang LT, Ma YH, Yang YQ, Lv YJ, Zhang ZC, et al. The biological fate of orally administered mPEG-PDLLA polymeric micelles. *J Control Release* 2020;**327**:725−36.

33. Li Y, Wang CL, Zong SY, Qi JP, Dong XC, Zhao WL, et al. The trigeminal pathway dominates the nose-to-brain transportation of intact polymeric nanoparticles: evidence from aggregation-caused quenching probes. *J Biomed Nanotechnol* 2019;**15**:686−702.

34. Xie YK, Shi BK, Xia F, Qi JP, Dong XC, Zhao WL, et al. Epithelia transmembrane transport of orally administered ultrafine drug particles evidenced by environment sensitive fluorophores in cellular and animal studies. *J Control Release* 2018;**270**:65−75.

35. Shen CY, Yang YQ, Shen BD, Xie YK, Qi JP, Dong XC, et al. Self-discriminating fluorescent hybrid nanocrystals: efficient and accurate tracking of translocation *via* oral delivery. *Nanoscale* 2018;**10**:436−50.

36. He HS, Xie YC, Lv YJ, Qi JP, Dong XC, Zhao WL, et al. Bioimaging of intact polycaprolactone nanoparticles using aggregation-caused quenching probes: size-dependent translocation *via* oral delivery. *Adv Healthc Mater* 2018;**7**:1800711.

37. Tan A, Colliat-Dangus P, Whitby CP, Prestidge CA. Controlling the enzymatic digestion of lipids using hybrid nanostructured materials. *ACS Appl Mater Interfaces* 2014;**6**:15363−71.

38. Kurihara A, Shibayama Y, Yasuno A, Ikeda M, Hisaoka M. Lipid emulsions of palmitoylrhizoxin: effects of particle size on blood dispositions of emulsion lipid and incorporated compound in rats. *Biopharm Drug Dispos* 1996;**17**:343−53.

39. USP monographs of Neoral® soft gelatin capsules. Available from, https://www.pharma.us.novartis.com/sites/www.pharma.us.novartis.com/files/neoral.pdf. [Accessed 4 September 2019].

40. Benito-Gallo P, Franceschetto A, Wong JC, Marlow M, Zann V, Scholes P, et al. Chain length affects pancreatic lipase activity and the extent and pH−time profile of triglyceride lipolysis. *Eur J Pharm Biopharm* 2015;**93**:353−62.

41. Qi JF, Jia CH, Shin JA, Woo JM, Wang XY, Park JT, et al. Effect of acylglycerol composition and fatty acyl chain length on lipid digestion in pH-stat digestion model and simulated *in vitro* digestion model. *J Food Sci* 2016;**81**:C317−23.

42. Zheng M, Chao C, Yu JL, Copeland L, Wang S, Wang SJ. Effects of chain length and degree of unsaturation of fatty acids on structure and *in vitro* digestibility of starch-protein-fatty acid complexes. *J Agric Food Chem* 2018;**66**:1872−80.

43. Hollis CP, Weiss HL, Evers BM, Gemeinhart RA, Li T. *In vivo* investigation of hybrid paclitaxel nanocrystals with dual fluorescent probes for cancer theranostics. *Pharm Res* 2014;**31**:1450−9.

44. Trevaskis NL, Kaminskas LM, Porter CJ. From sewer to saviour—targeting the lymphatic system to promote drug exposure and activity. *Nat Rev Drug Discov* 2015;**14**:781−803.

45. Liu JY, Werner U, Funke M, Besenius M, Saaby L, Fanø M, et al. SEDDS for intestinal absorption of insulin: application of Caco-2 and Caco-2/HT29 co-culture monolayers and intra-jejunal instillation in rats. *Int J Pharm* 2019;**560**:377−84.

46. Carlson TL, Lock JY, Carrier RL. Engineering the mucus barrier. *Annu Rev Biomed Eng* 2018;**20**:197−220.

47. Lock JY, Carlson TL, Carrier RL. Mucus models to evaluate the diffusion of drugs and particles. *Adv Drug Deliv Rev* 2018;**124**:34−49.

48. Beloqui A, Brayden DJ, Artursson P, Preat V, des Rieux A. A human intestinal M-cell-like model for investigating particle, antigen and microorganism translocation. *Nat Protoc* 2017;**12**:1387−99.

49. des Rieux A, Fievez V, Garinot M, Schneider YJ, Preat V. Nanoparticles as potential oral delivery systems of proteins and vaccines: a mechanistic approach. *J Control Release* 2006;**116**:1−27.

50. Brayden DJ, Jepson MA, Baird AW. Keynote review: intestinal Peyer's patch M cells and oral vaccine targeting. *Drug Discov Today* 2005;**10**:1145−57.